Nature of isomerism in exotic sulfur isotopes

Yutaka Utsuno,[1, 2, *] Noritaka Shimizu,[2] Takaharu Otsuka,[3, 2, 4] Tooru Yoshida,[2] and Yusuke Tsunoda[3]

[1] *Advanced Science Research Center, Japan Atomic Energy Agency, Tokai, Ibaraki 319-1195, Japan*
[2] *Center for Nuclear Study, University of Tokyo, Hongo, Bunkyo-ku, Tokyo 113-0033, Japan*
[3] *Department of Physics, University of Tokyo, Hongo, Bunkyo-ku, Tokyo 113-0033, Japan*
[4] *National Superconducting Cyclotron Laboratory, Michigan State University, East Lansing MI 48824, USA*

(Dated: December 31, 2014)

We clarify the origin of the anomalously hindered $E2$ decay from the 4_1^+ level in ^{44}S by performing a novel many-body analysis in the shell model. Within a unified picture about the occurrence of isomerism in neutron-rich sulfur isotopes, the 4_1^+ state is demonstrated to be a $K = 4$ isomer dominated by the two-quasiparticle configuration $\nu\Omega^\pi = 1/2^- \otimes \nu\Omega^\pi = 7/2^-$. The 4_1^+ state in ^{44}S is a new type of high-K isomer which has significant triaxiality.

PACS numbers: 21.60.Cs, 21.60.Ev, 21.10.Re, 27.40.+z

arXiv:1407.0444v2 [nucl-th] 30 Dec 2014

Among the most fundamental properties of nuclei is quadrupole collectivity, based on which the yrast 0^+, 2^+, 4^+, ... states in even-even nuclei are in general connected with strong $E2$ matrix elements. For open-shell nuclei in particular, $B(E2)$ values between neighboring yrast states are tens to hundreds of times larger than the Weisskopf estimate [1]. Contrary to this common sense, a recent experiment has reported [2] that the 4^+ state of ^{44}S located at 2.4 MeV, most likely the yrast state due to its small $E_x(4^+)$ to $E_x(2_1^+)$ ratio 1.9, has a strongly hindered $B(E2)$ value ($\lesssim 1$ W.u.) for the transition to 2_1^+. While this quite unusual $E2$ property of the 4_1^+ state, a kind of isomer, has been described with shell-model calculations [2], its underlying nuclear structure and lowering mechanism are still unclear. While a $K = 4$ high-K isomeric state is suggested in analogy to heavy-mass nuclei [2], this hypothesis is not supported by later microscopic calculations [3, 4].

Besides the 4_1^+ level in ^{44}S, plenty of exotic nuclear properties have been reported for neutron-rich sulfur isotopes. A modest $B(E2; 0_1^+ \to 2_1^+)$ value in ^{44}S [5] indicates the development of quadrupole collectivity despite the neutron magic number 28. An extraordinary low-lying isomeric 0_2^+ state in ^{44}S [6, 7] might suggest a spherical-deformed shape coexistence. Similarly, an isomeric $7/2_1^-$ state in ^{43}S is also possibly an indication of shape coexistence [8, 9]. Those observations have triggered state-of-the-art theoretical investigations based on the large-scale shell-model calculations [4, 10–13], the beyond-mean-field approaches [3, 14–16], and the antisymmetrized molecular dynamics (AMD) [17].

In this Letter, we demonstrate that the isomeric 4_1^+ state in ^{44}S occurs due to the dominance of a $K = 4$ intrinsic state by means of beyond-mean-field approximations to the shell model. We also present a unified understanding of the occurrence of the exotic isomers in neutron-rich sulfur isotopes ^{43,44}S, thus confirming the robustness of the present approaches and results. ^{44}S is the lightest-mass case among the high-K isomers ever identified in the $A \sim 100$, $A \sim 130$, $A \sim 180$, and $A \sim 250$ regions [18]. More surprisingly, this nucleus is triaxially deformed in contrast to the known cases having well-developed axially symmetric shapes [19].

We start with the conventional shell-model calculations for neutron-rich nuclei around $N = 28$ in the $\pi(sd)^{Z-8}\nu(pf)^{N-20}$ valence space with the SDPF-MU interaction [13]. As we will show in more detail later, the nuclear structure of the sulfur isotopes of the present interest is very well reproduced with the SDPF-MU interaction, as well as with the SDPF-U interaction [10].

While the shell-model calculation is capable of describing observables of nuclei quite quantitatively, it is not necessarily easy to draw a comprehensive picture of nuclear structure, in particular from the intrinsic-frame point of view. Introducing an appropriate mean-field based method into the shell model is a key to solving this problem. The method to be taken should represent spin-dependent intrinsic structure to describe the abrupt change between 2_1^+ and 4_1^+ in ^{44}S and should provide high-quality many-body wave functions comparable to the full shell-model calculation. Clearly, simple mean-field calculations such as the Hartree-Fock method cannot satisfy those demands. Here we take the variation after angular-momentum projection (AM-VAP) as a beyond-mean-field method to efficiently describe spin dependence within a framework that can well define an intrinsic state.

In the AM-VAP, wave functions are determined to minimize the energy $E(I\sigma) = \langle IM\sigma|H|IM\sigma\rangle_{\rm AM-VAP}/\langle IM\sigma|IM\sigma\rangle_{\rm AM-VAP}$ in the form of wave function

$$|IM\sigma\rangle_{\rm AM-VAP} = \sum_K g_K^{IM\sigma} \hat{P}^I_{MK} |\Phi(IM\sigma)\rangle, \qquad (1)$$

where $|\Phi(IM\sigma)\rangle = \prod_k \left(\sum_l D_{lk}^{IM\sigma} c_l^\dagger\right)|-\rangle$ is a general single Slater determinant parametrized by $D_{lk}^{IM\sigma}$ and can be regarded as the intrinsic state of $|IM\sigma\rangle_{\rm AM-VAP}$. $\hat{P}^I_{MK}$ is the usual angular-momentum projection operator [20] with I, M and K denoting the total angular momentum

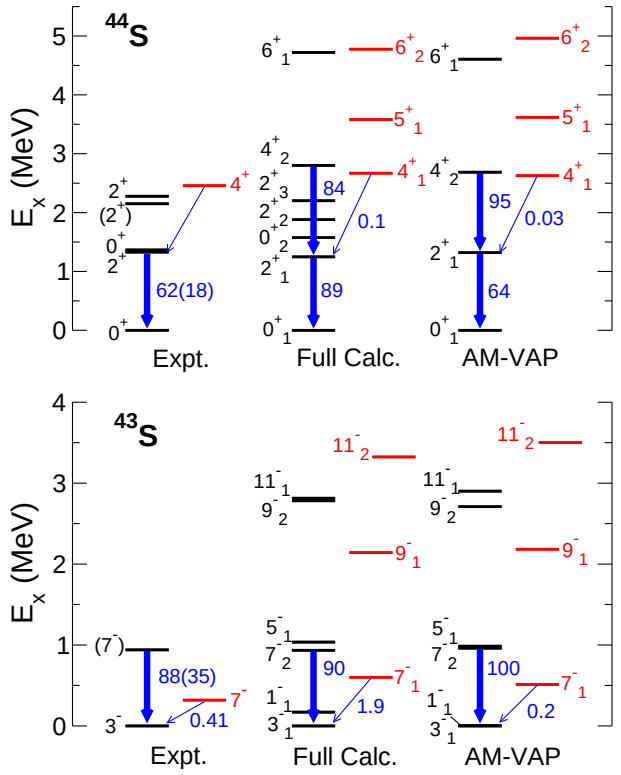

FIG. 1: (Color online) Energy levels and $B(E2)$ values (in $e^2\mathrm{fm}^4$) in ^{44,43}S compared among experiments (Expt.), the full shell-model calculation (Full Calc.), and the AM-VAP approximation to the shell model (AM-VAP). The spin-parity is denoted as J^π for ^{44}S and $2J^\pi$ for ^{43}S. Experimental data are taken from [2, 5, 6, 9, 23, 24].

and its z components along the laboratory and intrinsic frames, respectively, and each state with a given (I, M) is labeled with σ. The mixing of K in $|IM\sigma\rangle_{\mathrm{AM-VAP}}$ is represented by $g_K^{IM\sigma}$. $D_{lk}^{IM\sigma}$ and $g_K^{IM\sigma}$ are the variational parameters which are optimized using the conjugate gradient method [21] (see [22] for the expression of the gradient of $E(I\sigma)$). Furthermore, we calculate the overlap probabilities between the solutions found in this procedure and the shell-model wave functions of interest in order not to miss important solutions. Those overlap probabilities also work to test the quality of the AM-VAP wave functions. Multiple AM-VAP solutions, if found, are treated as separate levels if they are nearly orthogonal.

Figure 1 shows energy levels and $B(E2)$ values in ^{43,44}S compared among experiments, the full shell-model calculation, and the AM-VAP calculation. The $E2$ effective charges $(e_p, e_n) = (1.35e, 0.35e)$ are taken. As presented in Fig. 1, the results of the AM-VAP calculations are very close to those of the full shell-model calculations, including a strongly hindered $B(E2; 4_1^+ \to 2_1^+)$ value in ^{44}S. The overlap probabilities calculated between the full shell-model states and the AM-VAP states are rather

TABLE I: Distribution of $|K|$ and deformation parameters (β, γ) (γ: in deg.) in the AM-VAP states for ^{44}S.

I_σ^π	$\lvert K\rvert$							β	γ
	0	1	2	3	4	5	6		
0_1^+	1.00							0.24	33
2_1^+	0.98	0.00	0.01					0.26	23
4_2^+	0.92	0.08	0.00	0.00	0.00			0.28	14
6_1^+	0.76	0.23	0.01	0.00	0.00	0.00	0.00	0.28	13
4_1^+	0.00	0.00	0.00	0.07	0.93			0.23	28
5_1^+	0.00	0.00	0.01	0.08	0.85	0.07		0.23	24
6_2^+	0.00	0.01	0.01	0.14	0.80	0.04	0.00	0.23	26

TABLE II: Same as TABLE I but for ^{43}S.

I_σ^π	$\lvert K\rvert$						β	γ
	1/2	3/2	5/2	7/2	9/2	11/2		
$1/2_1^-$	1.00						0.27	15
$3/2_1^-$	0.98	0.02					0.25	17
$5/2_1^-$	0.97	0.03	0.00				0.27	16
$7/2_2^-$	0.96	0.04	0.00	0.00			0.25	16
$9/2_2^-$	0.96	0.04	0.00	0.00	0.00		0.28	15
$11/2_1^-$	0.91	0.09	0.00	0.00	0.00	0.00	0.25	16
$7/2_1^-$	0.00	0.01	0.01	0.98			0.22	31
$9/2_1^-$	0.00	0.01	0.04	0.95	0.01		0.23	31
$11/2_2^-$	0.00	0.01	0.01	0.08	0.03	0.87	0.25	37

close to unity: 0.92, 0.81, 0.86, 0.88, and 0.90 for the 0_1^+, 2_1^+, 4_1^+, 4_2^+, and 5_1^+ states in ^{44}S, respectively, and 0.96, 0.91, 0.85, 0.93, 0.93, 0.92, 0.93, 0.92, and 0.84 for the $1/2_1^-$, $3/2_1^-$, $5/2_1^-$, $7/2_1^-$, $7/2_2^-$, $9/2_1^-$, $9/2_2^-$, $11/2_1^-$, and $11/2_2^-$ states in ^{43}S, respectively. The 6^+ states of the AM-VAP split into the two shell-model states because of the accidental degeneracy of the 6^+ states in the shell-model calculation.

Supported by those very large overlaps, it is reasonable to deduce intrinsic properties of many-body wave functions from the corresponding AM-VAP intrinsic states, $|\Phi(IM\sigma)\rangle$ in Eq. (1). The intrinsic mass quadrupole moments Q_0 and Q_2 are given as the expectation values of the mass quadrupole operators r^2Y_{20} and r^2Y_{22} in $|\Phi(IM\sigma)\rangle$, respectively, where the axes of the intrinsic frame are determined to diagonalize the quadrupole tensor and to satisfy the order $\langle Q_{zz}\rangle \geq \langle Q_{xx}\rangle \geq \langle Q_{yy}\rangle$. It is noted that a similar method has been used to deduce shape fluctuation in exotic Ni isotopes from the Monte Carlo shell-model wave functions [25]. The quadrupole deformation parameters (β, γ) are then defined in the usual way as $\beta = f_{\mathrm{scale}}\sqrt{\frac{5}{16\pi}}\frac{4\pi}{3R^2A}\sqrt{(Q_0)^2 + 2(Q_2)^2}$ and $\gamma = \arctan(\frac{\sqrt{2}Q_2}{Q_0})$, with $R = 1.2A^{1/3}$ fm [26]. Here, a factor $f_{\mathrm{scale}} = e_p/e + e_n/e$ is introduced to rescale quadrupole matrix elements between the shell-model space and the full single-particle space. Since the intrinsic axes are thus determined, the K quantum number is well defined apart from its sign. The distribution of K,

which is normalized to unity, is calculated by following the method shown in Ref. [26].

The intrinsic properties of the AM-VAP states defined above are listed in Table I and Table II for ^{44}S and ^{43}S, respectively. We first outline the properties of ^{44}S. The 0_1^+, 2_1^+, 4_2^+, 6_1^+ sequence, connected with strong $E2$ matrix elements, is dominated by the $K = 0$ state as usually conceived for the ground-state band, whereas the $K = 1$ component grows up with increasing spin because of the Coriolis coupling. The shape of the ground-state band evolves from triaxial to prolate. This shape evolution is very similar to the results of a beyond-mean-field calculation based on the GCM [3] and an analysis based on the quadrupole rotational invariants in the shell-model wave functions [4]. On the other hand, the 4_1^+, 5_1^+, 6_2^+ sequence, also connected with strong $E2$ matrix elements, is missing in the beyond-mean-field study of Ref. [3], but appears in the shell model both with the SDPF-U interaction [2, 4] and with the SDPF-MU interaction [13].

The present AM-VAP calculation demonstrates that this band is strongly dominated by the $K = 4$ state for the first time. Experimentally, while this K assignment has been suggested in [2], its basis is only the weak $E2$ transition to the 2_1^+ level because the usual shell-model calculation cannot provide K quantum numbers. In light nuclei, however, such a high-K isomer has not been known and is rather unexpected. It is commonly believed that the high-K isomerism occurs only in axially symmetric, stably deformed nuclei [19], whereas this condition is not satisfied in light nuclei. What is surprising in the present case is that the the concentration of the K numbers takes place in the $K = 4$ band in spite of the significant triaxiality of the $K = 4$ states. The AM-VAP calculation shows that although the K numbers are strongly mixed in the intrinsic state $|\Phi\rangle$ of Eq. (1), the purity of K is approximately restored after diagonalizing the Hamiltonian in the K space.

Why does the $K = 4$ band emerge at such a low excitation energy in ^{44}S? The structure of ^{43}S brings key information on this question, which we briefly examine here. The energy levels in ^{43}S are presented in Fig. 1 and their intrinsic properties are listed in Table II. The observed energy levels and the $E2$ transitions are well reproduced with the full shell-model and AM-VAP calculations. The strong $E2$ excitation to the 940 keV state [24] and the isomeric state at 320 keV [8, 9], shown in Fig. 1, suggest a possible coexistence of configurations. While the ground state should be deformed on the basis of the large $B(E2; \text{g.s.} \rightarrow 940\,\text{keV})$ value, the structure of $7/2_1^-$ has been less understood. Although an early analysis [9] proposed a quasi-spherical state, the large quadrupole moment in this state measured later [27], $|Q| = 23(3)\ e\text{fm}^2$, casts doubt on this interpretation. The AM-VAP analysis demonstrates that the ground state and the $7/2_1^-$ state are dominated by $K = 1/2$ and $K = 7/2$, respectively, and that this K forbiddeness causes the isomerism in

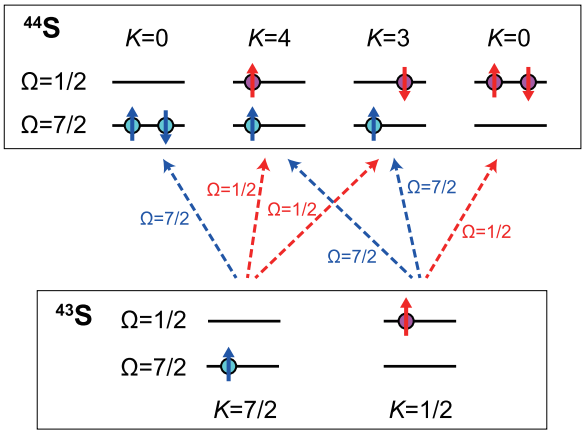

FIG. 2: (Color online) Possible low-lying neutron configurations for ^{44}S and ^{43}S.

$7/2_1^-$. Although this result is consistent with the suggestion of [17], the present calculation is the first to quantitatively provide the distribution of K. The $K = 7/2$ and $K = 1/2$ states have triaxial and nearly prolate deformations, respectively, in accordance with [4, 17]. Thus, similar to the $K = 4$ band in ^{44}S, the $K = 7/2$ band in ^{43}S has an approximately good K number in spite of the development of triaxiality.

Since ^{43}S is an even-odd nucleus, the K quantum number is determined by that of the unpaired neutron, Ω^π. On the basis of the above analysis, we hereafter assume a good Ω^π quantum number even in the case of non axially-symmetric deformation. As expected from the Nilsson diagram (see also Ref. [17]), the orbit of the last neutron can be $\Omega^\pi = 1/2^-$ which favors prolate deformation or $\Omega^\pi = 7/2^-$ which favors oblate deformation. Thus, the $K = 1/2$ state favors a prolate shape because of the preference of prolate deformation for both the $\Omega^\pi = 1/2^-$ neutron and the ^{42}S core (see the potential energy surface of ^{42}S, e.g., in Ref. [13]). The $K = 7/2$ state, on the other hand, is inclined to be triaxial due to the opposite shape preference between the last neutron and the core.

Now we turn to ^{44}S. It is reasonable to fix the ^{42}S core and to take into account only the two quasiparticle degrees of freedom, $\Omega^\pi = 1/2^-$ and $7/2^-$. It is noted that the quasiparticle state is introduced, as usual, to include pairing correlation within the single-particle picture. Those two orbits are regarded to be nearly degenerate in this simple picture similarly to the small energy difference between the $3/2_1^-$ and $7/2_1^-$ states in ^{43}S. For the two-quasiparticle system of ^{44}S, two $K = 0$ states, one $K = 3$ state, and one $K = 4$ state can be constructed by adding a neutron as illustrated in Fig. 2. We then consider the competition of energy between different K states by decomposing the energy of a state into the intrinsic energy and the rotational energy. Concerning the intrinsic energy, the lowest $K = 0$ zero-quasiparticle

state is in general lower than the $K \neq 0$ two-quasiparticle states even if the relevant quasiparticle states are degenerate because the former gains additional energy due to pairing, which amounts to 2Δ, where Δ is the pairing gap. Thus, the $K = 0$ state usually dominates the yrast $0^+, 2^+, 4^+, \ldots$ sequence. High-K states are, however, advantageous over the $K = 0$ state in terms of the loss of the rotational energy $E_{\rm rot} = (\hbar^2/2\mathcal{I})(I(I+1) - K^2)$, which is smaller for high-K states. This is the standard picture for the occurrence of high-K isomers seen usually in the medium-heavy-mass or heavy-mass regions [28]. In those heavier-mass regions, the $K \neq 0$ states cannot be lower than the $K = 0$ member unless K is sufficiently large because moments of inertia are rather large. On the other hand, for lighter nuclei with relatively small moments of inertia, a state with a modest K can, in principle, intrude into the yrast $0^+, 2^+, 4^+, \ldots$ sequence if a high-Ω orbit is located very close to the Fermi surface. ^{44}S is such a very rare case, but similar situations can occur in other nuclei. For nuclei around ^{44}S, two quasiparticle states are estimated to appear above $2\Delta \approx 2.5$ MeV, where the pairing gap is evaluated from one-neutron separation energies of ^{43,44,45}S. This energy estimate accounts for the excitation energy of the measured isomeric 4^+ state. On the other hand, the 4^+ state with $K = 0$ is roughly estimated to lie around 3 MeV by assuming a normal $E_x(4^+)/E_x(2^+)$ ratio, ~ 2.5. This is how the $K = 4$ state becomes the yrast state in ^{44}S when $\Omega^\pi = 7/2^-$ and $\Omega^\pi = 1/2^-$ are nearly degenerate.

In the beyond-mean-field approach of Ref. [3], the low-lying $K = 4$ state is missing despite many other similarities, such as shapes, to the present calculations. This is due to the restriction of time-reversal symmetry on the intrinsic states imposed in the calculation of Ref. [3]. The AM-VAP calculation in fact demonstrates that the time-reversal symmetry is almost completely broken for the intrinsic state of the $K = 4$ state. The overlap probabilities between $|\Phi\rangle$ of Eq. (1) and its time-reversed state $\mathcal{T}|\Phi\rangle$ are calculated to be only 0.02-0.08 for the $K = 4$ members. The breaking of time-reversal symmetry in the intrinsic state is almost solely attributed to the neutron part of the wave function.

Here we confirm that the actual shell-model wave function of 4^+_1 is indeed dominated by the above-mentioned two-quasiparticle state by calculating its spectroscopic strengths. The full shell-model calculation leads to large overlap probabilities of the 4^+_1 state with the $\mathcal{A}[\nu p_{3/2} \otimes 7/2^-_1]^{J=4}$ and $\mathcal{A}[\nu f_{7/2} \otimes 7/2^-_2]^{J=4}$ states (0.66 and 0.54, respectively), where $\mathcal{A}$ denotes antisymmetrization and normalization. On the other hand, its overlap probabilities with $\mathcal{A}[\nu f_{7/2} \otimes 7/2^-_1]^{J=4}$ and $\mathcal{A}[\nu p_{3/2} \otimes 7/2^-_2]^{J=4}$ are much smaller (0.19 and 0.00, respectively). This is a direct consequence of the dominance of the configurations illustrated in Fig. 2, since the $7/2^-_1$ and $7/2^-_2$ states are dominated by $K = 7/2$ and $K = 1/2$, respectively, and the $\Omega^\pi = 1/2^-$ and $\Omega^\pi = 7/2^-$ single-particle states are dominated by $p_{3/2}$ and $f_{7/2}$, respectively.

We also point out that the configurations shown in Fig. 2 account for the reason why the 0^+_2 state in ^{44}S lies extraordinary low. In Fig. 2, two $K = 0$ states exist, having similar diagonal energies. The off-diagonal Hamiltonian matrix element between those $K = 0$ states strongly mixes and repels each other, but the excited $K = 0$ state can be rather low if the two quasiparticle states are nearly degenerate. The strong mixing between those two $K = 0$ states is supported by the shell-model result that the overlap probability of the 0^+_1 state with $\mathcal{A}[\nu f_{7/2} \otimes 7/2^-_1]^{J=0}$ (0.61) is close to the one with $\mathcal{A}[\nu p_{3/2} \otimes 3/2^-_1]^{J=0}$ (0.39). When the total spin for each $K = 0$ state increases, the state with a larger moment of inertia is relatively lowered. Here, the $K = 0$ state that occupies $\Omega^\pi = 1/2^-$ is the case because of larger, prolate deformation. This accounts for the shape evolution toward prolate deformation within the $K = 0$ band shown in Table I. It is noted that the ground state and $K = 4$ states deviate from a prolate shape because they occupy the oblate-favored $\Omega^\pi = 7/2^-$ orbit.

Finally, we note that the $K = 3$ state illustrated in Fig. 2 is also found in the shell-model and AM-VAP calculations. In the shell-model calculation, the 3^+_1 level appears very close to 4^+_1, dominated by the $K = 3$ AM-VAP state. The $K = 3$ states are distinguishable from the $K = 4$ states by neutron intrinsic-spin expectation value because of difference in neutron spin orientation.

In conclusion, we have clarified that the isomeric 4^+_1 state in ^{44}S observed recently [2] originates from the dominance of the $K = 4$ state by means of the variation after angular-momentum projection (AM-VAP) approximation to the shell model. This result is very robust because it is understood within a unified picture about the occurrence of exotic isomeric states in ^{43,44}S including the $7/2^-_1$ state in ^{43}S and the 0^+_2 in ^{44}S. The $K = 4$ state is missing in the beyond-mean-field calculation [3] due to the restriction of time-reversal symmetry and may appear without it. Having extraordinary light mass and triaxial deformation, the $K = 4$ isomer in ^{44}S is distinct from previously known high-K isomers. Thus, the possibility of the occurrence of high-K isomerism is greatly extended to the whole chart of nuclides, which provides new experimental and theoretical opportunities.

Y. U. thanks Prof. I. Wiedenhöver for his enlightening discussions at an early stage and Dr. T. Shizuma for useful comments on high-K isomers. The conventional shell-model calculations were performed with the code MSHELL64 [29], and the AM-VAP calculations were carried out with the advanced Monte-Carlo shell-model code [22]. This work was supported in part by JSPS KAKENHI Grant Numbers 20244022, 21740204, and 25870168. This work has been supported by HPCI (hp120284 and hp130024), and is a part of the RIKEN-CNS joint research project on large-scale nuclear-structure calculations.

* Electronic address: utsuno.yutaka@jaea.go.jp

[1] For instance, A. Bohr and B. R. Mottelson, *Nuclear Structure*, Vol. II, Benjamin, New York, 1975.
[2] D. Santiago-Gonzalez *et al.*, Phys. Rev. C **83**, 061305(R) (2011).
[3] T. R. Rodríguez and J. L. Egido, Phys. Rev. C **84**, 051307(R) (2011).
[4] R. Chevrier and L. Gaudefroy, Phys. Rev. C **89**, 051301(R) (2014).
[5] T. Glasmacher *et al.*, Phys. Lett. B **395**, 163 (1997).
[6] S. Grévy *et al.*, Eur. Phys. J. A **25**, 111 (2005).
[7] C. Force *et al.*, Phys. Rev. Lett. **105**, 102501 (2010).
[8] F. Sarazin *et al.*, Phys. Rev. Lett. **84**, 5062 (2000).
[9] L. Gaudefroy *et al.*, Phys. Rev. Lett. **102**, 092501 (2009); P.F. Mantica, Physics **2**, 18 (2009).
[10] F. Nowacki and A. Poves, Phys. Rev. C **79**, 014310 (2009).
[11] L. Gaudefroy, Phys. Rev. C **81**, 064329 (2010).
[12] K. Kaneko, Y. Sun, T. Mizusaki, and M. Hasegawa, Phys. Rev. C **83**, 014320 (2011).
[13] Y. Utsuno, T. Otsuka, B. A. Brown, M. Honma, T. Mizusaki, and N. Shimizu, Phys. Rev. C **86**, 051301(R) (2012).
[14] S. Péru, M. Girod, and J. F. Berger, Eur. Phys. J. A **9**, 35 (2000).
[15] R. Rodríguez-Guzmán, J. L. Egido, and L. M. Robledo, Phys. Rev. C **65**, 024304 (2002).
[16] Z. P. Li, J. M. Yao, D. Vretenar, T. Nikšić, H. Chen, and J. Meng, Phys. Rev. C **84**, 054304 (2011).
[17] M. Kimura, Y. Taniguchi, Y. Kanada-En'yo, H. Horiuchi, and K. Ikeda, Phys. Rev. C **87**, 011301(R) (2013).
[18] P. M. Walker, AIP Conf. Proc. **819**, 16 (2006).
[19] P. M. Walker and G. D. Dracoulis, Nature **399**, 35 (1999).
[20] P. Ring and P. Schuck, *The Nuclear Many-Body Problem*, Springer-Verlag, Berlin, 1980.
[21] W. H. Press, S. A. Teukolsky, W. T. Vetterling, and B. P. Flannery, *Numerical Recipes in FORTRAN 77: The Art of Scientific Computing*, Second Edition, Cambridge University Press, Cambridge, 1992.
[22] N. Shimizu, T. Abe, Y. Tsunoda, Y. Utsuno, T. Yoshida, T. Mizusaki, M. Honma, and T. Otsuka, Prog. Theor. Exp. Phys. **2012**, 01A205 (2012).
[23] L. Cáceres *et al.*, Phys. Rev. C **85**, 024311 (2012).
[24] R. W. Ibbotson, T. Glasmacher, P. F. Mantica, and H. Scheit, Phys. Rev. C **59**, 642 (1999).
[25] Y. Tsunoda, T. Otsuka, N. Shimizu, M. Honma, and Y. Utsuno, Phys. Rev. C **89**, 031301(R) (2014).
[26] T. R. Rodríguez and J. L. Egido, Phys. Rev. C **81**, 064323 (2010).
[27] R. Chevrier *et al.*, Phys. Rev. Lett. **108**, 162501 (2012).
[28] For instance, P. M. Walker and G. D. Dracoulis, Hyperfine Int. **135**, 83 (2001).
[29] T. Mizusaki, N. Shimizu, Y. Utsuno, and M. Honma, MSHELL64 code (unpublished).